Combination of free-space and guided-wave optical interconnects for angularly multiplexed multiwavelength holographic memory

De-Gui Sun, Richard Lee, and Ray T. Chen

We propose and test experimentally a new scheme to implement spatially multiplexed multiwavelength holographic memory. An electro-optically modulated phase grating array on $LiNbO_3$ substrate is used as a guided-wave interconnect to activate the reconfigurable reference beam. The object beam is provided by free-space interconnect. An electro-optic modulation efficiency of $18 \pm 2.5°$ is achieved with an applied voltage of 100 V. The reference beams with different diffraction angles can implement the angle-multiplexing holographic recording. We believe this is the first report of the implementation of guided-wave electro-optic interconnect together with free-space interconnect in holographic memory applications. © 1997 Optical Society of America

Key words: Guided-wave interconnect, free-space interconnect, electro-optically modulated phase grating array, modulation efficiency, holographic memory, angle multiplexing.

1. Introduction

High-capacity programmable holographic memories without any moving parts have long been considered a feasible solution for upgrading performance of the memory density and the access time.[1–5] Also, the multiplexibility of the holographic medium plays an important role in realizing high-density holographic memories.[5–16] To date, the most widely investigated multiplexing approaches are wavelength,[5–9] angle,[8–11] shift,[12,13] and phase.[14,15] Among these multiplexing approaches, the wavelength and the angle multiplexings seem to be most promising.[5–11] More recently, combinations of these multiplexing approaches are beginning to receive much attention.[8,9,13,16] In particular, the combination of angle multiplexing and wavelength multiplexing has become the focused point of the hybrid multiplexings for improving the performances of high-density optical memories.[8,9]

For volume phase grating materials, where large index modulation and therefore information multiplexibility are reported,[17,18] Bragg-grating-based multiple fan-out interconnects can be realized with a single fan-out node.[19,20] For a thin phase grating, where interaction length is short, one-to-many fan-out can still be realized in the Raman–Nath regime.[21,22] In this case the energy distribution of multiple fan-outs is correlated so that minimization of power fluctuations among multiple diffraction orders is a paramount issue for carrying out the required fan-out involving multiple diffraction orders with a minimum power budget. We report on a multiplexed holographic memory that makes use of free-space object beams and guided-wave reference beams. A $LiNbO_3$-based electro-optic (EO) phase grating array with a reconfigurable multi-fan-out capability is investigated. The reference beam is generated through the electro-optically modulated phase grating array and the object beam is introduced by free-space interconnect. On the basis of this scheme, we studied angle-multiplexing holographic recording using different diffraction orders with different diffraction angles to provide the reference beams while we were able to implement the wavelength-multiplexing recording by changing the laser wavelength for the holographic recording at each location. The recording medium we used was Dupont photopolymer film because of its superior wavelength and angular sensitivity.[23]

2. Analysis for Massive Fan-Out of Electro-Optic Grating

A schematic of the modulated phase grating aimed at achieving multiple fan-outs from the waveguide sub-

The authors are with the Department of Electrical and Computer Engineering, The University of Texas at Austin, Austin, Texas 78712-1084.

Received 24 March 1997; revised manuscript received 24 April 1997.

0003-6935/97/328329-07$10.00/0

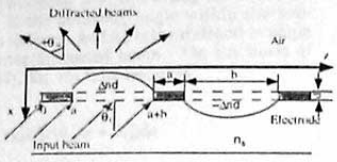

Fig. 1. Diffraction schematic of modulated thin phase grating; $a = 2$ μm and $b = 6$ μm.

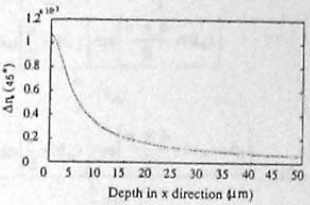

Fig. 2. Distribution curve of index modulation as a function of x.

strate is illustrated in Fig. 1. The voltage applied to the interdigitated electrodes associated with an x-cut $LiNbO_3$ crystal induces a periodic index modulation.[24,25] The effective value of this periodic index modulation Δn_{eff} determines the optical path difference along the x axis, i.e., $\Delta n_{\text{eff}}d$, where d is the depth of index modulation (see Fig. 1). The relation between the index modulation and the depth in x axis depends on the incident angle θ_1 of the light in the crystal and the modulation electric field as depicted by[25]

$$\Delta n_e(\theta_1) = \frac{n_e^3 \sin^2\theta_1 \Delta n_o - n_o^3 \cos^2\theta_1 \Delta n_e}{(n_o^2\cos^2\theta_1 - n_e^2\sin^2\theta_1)^{3/2}}, \quad (1)$$

where E_z is the component of modulation electric field in z direction, and Δn_e and Δn_o are calculated by the following set:

$$\Delta n_e = -\frac{1}{2} n_e^3 \gamma_{33} E_z, \quad (2a)$$

$$\Delta n_o = -\frac{1}{2} n_o^3 \gamma_{13} E_z, \quad (2b)$$

where γ_{33} and γ_{13} are the EO coefficients of the $LiNbO_3$ gratings. Because only the coupling case in x direction is studied, we can set the z value to zero when we discuss the index modulation in x direction. By combining Eqs. (1), (2a), and 2(b) and taking $\theta_1 = 45°$, we obtain the index modulation curve $\Delta n_e(45°, x)$ with respect to x, as shown in Fig. 2. Note that the index modulation, $\Delta n_e(45°, x)$, decreases dramatically along x (depth) direction. Thus the effective optic path difference $\Delta n_{\text{eff}}d$ should be calculated by[25]

$$\Delta n_{\text{eff}}d = \int_{-d_e}^{0} \Delta n_e(\theta_1, x)\,dx, \quad (3)$$

where d_e is called the effective modulation depth at which the index modulation is $1/e$ of the value at $x = 0$; whereas along the direction of the grating vector, i.e., z axis, the effective optic path difference $\Delta n_{\text{eff}}d$ can be defined by

$$\Delta n_{\text{eff}}d = \begin{cases} 0 & (0 < z \le a) \\ \Delta n_{\text{eff}}d & (a < z \le a + b) \\ 0 & (a + b < z \le 2a + b) \\ -\Delta n_{\text{eff}}d & (2a + b < z \le 2a + 2b) \end{cases} \quad (4)$$

With Eq. (4) we obtain the distribution pattern of the effective optic path difference $\Delta n_{\text{eff}}d$ along z axis as shown in Fig. 3. It is clear that the thin phase grating generated through index modulation has a period $\Lambda = 2(a + b)$. With the input intensity set as 1, the complex amplitude distribution of a light wave from a single period that resulted from refractive index perturbation can be described by[26]

$$E_1 = \sum_{z_i}^{\infty} \frac{1}{Z_i} \int_0^{z_i} \exp[ik\Delta L_i(z)]\,dz, \quad (5)$$

where $k = 2\pi/\lambda$ is the wave vector of the incident light, λ is the wavelength, z_i is the ith definition range of the phase function of the grating, and $L_i(z)$ is defined by

$$\Delta L_i(z) = \begin{cases} \dfrac{r(\theta_m)z + \delta_1}{k} & (0 < z \le a) \\ \dfrac{r(\theta_m)z + \delta_2}{k} & (a < z \le a + b) \\ \dfrac{r(\theta_m)z + \delta_1}{k} & (a + b < z \le 2a + b) \\ \dfrac{r(\theta_m)z - \delta_2}{k} & (2a + b < z \le 2a + 2b) \end{cases}, \quad (6)$$

$$r(\theta_m) = (n_z \sin\theta_1 + n_2 \sin\theta_m)k, \quad (7a)$$

$$\delta_1 = kn_1 \cos\theta_1, \quad (7b)$$

$$\delta_2 = k\Delta n_e(\theta_1)d/\cos\theta_1. \quad (7c)$$

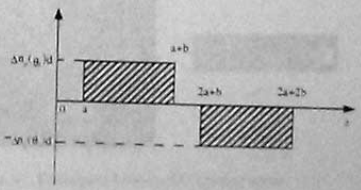

Fig. 3. Distribution pattern of modulated effective optical path difference along z axis.

In Eqs. (7a) through (7c), n_1 and n_2 are the indices of the electrode material and the filling material, respectively; θ_1 is the bouncing angle within the substrate with an index n_s; and θ_m is the diffraction angle of the mth-order diffracted beam. On the basis of Eqs. (6) and (7), Eq. (5) thus becomes

$$
\begin{aligned}
E_1(\theta_m) = {} & \frac{1}{a}\int_0^a \exp\{i[r(\theta_m)z + \delta_1]\}dz \\
& + \frac{1}{b}\int_a^{a+b} \exp\{i[r(\theta_m)z + \delta_2]\}dz \\
& + \frac{1}{a}\int_{a+b}^{2a+b} \exp\{i[r(\theta_m)z + \delta_1]\}dz \\
& + \frac{1}{b}\int_{2a+b}^{2a+2b} \exp\{i[r(\theta_m)z - \delta_2]\}dz \\
= {} & \frac{\{\exp[iar(\theta_m)] - 1\}\exp(i\delta_1)}{iar(\theta_m)} \\
& - \frac{\{\exp[ibr(\theta_m)] - 1\}\exp\{i[ar(\theta_m) - \delta_2]\}}{ibr(\theta_m)} \\
& - \frac{\{\exp[iar(\theta_m)] - 1\}\exp\{i[(a+b)r(\theta_m) + \delta_1]\}}{iar(\theta_m)} \\
& - \frac{\{\exp[ibr(\theta_m)] - 1\}\exp\{i[(2a+b)r(\theta_m) - \delta_2]\}}{ibr(\theta_m)} \\
= {} & \frac{4}{ar}\sin\left[\frac{a}{2}r(\theta_m)\right]\cos\left[\frac{a+b}{2}r(\theta_m)\right] \\
& \times \exp\left\{i\left[\frac{2a+b}{2}r(\theta_m) + \delta_1\right]\right\} \\
& - \frac{4}{br}\sin\left[\frac{b}{2}r(\theta_m)\right]\cos\left[\frac{a+b}{2}r(\theta_m) - \delta_2\right] \\
& \times \exp\left[i\,\frac{3a+2b}{2}r(\theta_m)\right]. \qquad (8)
\end{aligned}
$$

From Eq. (8), the intensity distribution of a normalized diffraction from a single grating period can be represented as

$$
\begin{aligned}
I_1(\theta_m) = {} & E_1 \cdot E_1^* \\
= {} & \left\{\frac{2\sin\left[\frac{a}{2}r(\theta_m)\right]\cos\left[\frac{a+b}{2}r(\theta_m)\right]}{\frac{a}{2}r(\theta_m)}\right\}^2 \\
& + \left\{\frac{2\sin\left[\frac{b}{2}r(\theta_m)\right]\cos\left[\frac{a+b}{2}r(\theta_m) - \delta_2\right]}{\frac{b}{2}r(\theta_m)}\right\}^2 \\
& + 2\cos\left[\frac{a+b}{2}r(\theta_m) - \delta_1\right] \\
& \times \frac{2\sin\left[\frac{a}{2}r(\theta_m)\right]\cos\left[\frac{a+b}{2}r(\theta_m)\right]}{\frac{a}{2}r(\theta_m)} \\
& \times \frac{2\sin\left[\frac{b}{2}r(\theta_m)\right]\cos\left[\frac{a+b}{2}r(\theta_m) - \delta_2\right]}{\frac{b}{2}r(\theta_m)}. \qquad (9)
\end{aligned}
$$

Furthermore, according to the principle of grating diffraction, the intensity distribution of a normalized multislit diffraction can be represented as

$$
I_2(\theta_m) = \left\{\frac{\sin\left[\frac{N\Lambda r(\theta_m)}{2}\right]}{\sin\left[\frac{\Lambda r(\theta_m)}{2}\right]}\right\}^2, \qquad (10)
$$

where N is the total number of grating grooves. Combining Eqs. (9) and (10), we have the final normalized intensity distribution[26]:

$$
I(\theta_m) = \sum_m I_1(\theta_m) \cdot I_2(\theta_m). \qquad (11)
$$

3. Experiments and Discussions

The experimental study here contains two parts. The first part concerns the multiple fan-out performance of the EO phase grating array, and the second part concerns the recording and reading of an angularly multiplexed multiwavelength holographic plane image. Here $\theta_1 = 45°$ is required to satisfy the total-internal-reflection condition for waveguiding within the $LiNbO_3$ substrate, and the refractive index n_s of the $LiNbO_3$ crystal is a function of the incident angle θ_1.[27] With $n_o = 2.29$ and $n_e = 2.20$, we obtain $n_s = 2.24$, corresponding to $\theta_1 = 45°$.[28] With other parameters such as $\lambda = 0.633\ \mu m$, $a = 2\ \mu m$, $b = 6\ \mu m$, $N = 60$, $n_1 = 2.099$, $n_2 = 2.086$, $r_{33} = 30.9 \times 10^{-12}$, $r_{13} = 9.6 \times 10^{-12}$, and $V = 100$ V, we obtain the effective modulation depth $d_e = 8\ \mu m$ and $\Delta n_{eff} d \approx 1.68 \times 10^{-3}\ \mu m$. The fabricated $LiNbO_3$ EO grating

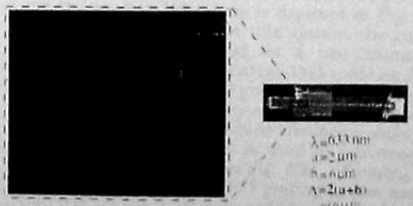

Fig. 4. Fabricated $LiNbO_3$ EO grating array

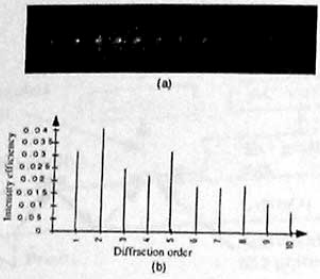

Fig. 5. Angular distribution of multiple diffraction orders coupled by EO modulated grating: (a) far-field pattern of multiple diffraction orders, (b) measured result, (c) theoretical result; θ_m represents the output angle associated with the mth diffraction order.

array is shown in Fig. 4, where the detailed microstructure associated with each grating is also included. The grating was made from an indium tin oxide film coated on an x-cut $LiNbO_3$ substrate. The observed fan-out and the measured values of various diffraction orders that correspond to the above-mentioned experimental setting are illustrated in Figs. 5(a) and 5(b), respectively. The θ_m-dependent distribution for the final normalized intensity is shown in Fig. 5(c). Note that the measured result of the EO grating diffraction shown in Fig. 5(b) agrees with the calculated result shown in Fig. 5(c). Because this multiple fan-out EO grating is used to provide a multiwavelength programmable holographic memory, the relation between the diffraction angle θ_m and wavelength λ is worthy of special discussion for each diffraction order. According to Eq. (10), the condition that produces the mth-order diffraction peak can be described by

$$\Lambda \cdot r(\theta_m) = 2m\pi. \tag{12}$$

Combining Eqs. (7a) and (12), we have

$$\theta_m = \sin^{-1}\left[\frac{1}{n_2}\left(\frac{m\lambda}{\Lambda} - n_s \sin\theta_i\right)\right]. \tag{13}$$

The distribution of diffraction angles with respect to the wavelength defined by Eq. (13) is shown in Fig. 6. Comparing the curves of Fig. 6 with that of Fig. 5, we found that some diffraction orders of the multiperiod diffraction defined by Eq. (12) vanished after the multiperiod diffraction combined with the single-period

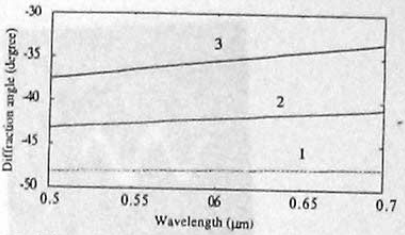

Fig. 6. Relationship between θ_m and λ of three different diffraction orders: 1, the first order; 2, the fifth order; 3, the tenth order.

diffraction. Namely, the total diffraction orders were less than that of the multiperiod diffraction defined by Eq. (12). Note further that the diffraction angle is almost uniform with the wavelength for a given diffraction order, which is somewhat helpful for the multiwavelength recording at one location.

If the nth EO grating spot is activated, the measured modulation efficiency of the mth diffraction order is defined by[9]

$$\eta_{lm} = \frac{P_m(n)}{P_t(n) - P_l(n)}, \tag{14}$$

where $P_m(n)$ is the power of the mth diffracted beam after the applied voltage is activated, $P_t(n)$ is the total power of the substrate guided wave before it interacts with the EO grating, and $P_l(n)$ is the power loss within the substrate. Both $P_t(n)$ and $P_l(n)$ are influenced mainly by the background grating effect whereas $P_m(n)$ is determined by the modulation efficiency of $LiNbO_3$ and the structure of the EO grating. The experimental setup for ac measurement is shown in Fig. 7(a). A pair of test-probe positioners is used to apply the modulation voltage onto the EO gratings. Reconfiguration of the fan-out beams is realized experimentally through the activation of each EO grating independently. The observed experimental result of the EO grating diffraction is given in Fig. 7(b), which represents a $18 \pm 2.5\%$ modulation efficiency at 100 volts. This is well matched with theoretical predictions.

The proposed configuration for successively recording and reading holograms is depicted in Figs. 8(a) and 8(b), respectively. In this system, the guided-wave interconnects based on a one-dimensional $LiNbO_3$-based EO grating array that contains 30 individually addressable EO gratings are used to introduce the reference beam through the total internal reflections with a predetermined bouncing angle, and free-space interconnection is used to introduce the object beam. As shown in Fig. 8(b), a focusing lens that corresponds to each EO grating is also used to converge all the diffraction orders onto one memory spot. The focal length f_l determines the separation S between the waveguide and the hologram plate (i.e., $S \approx 2f_l$). In addition, a polarized beam splitter

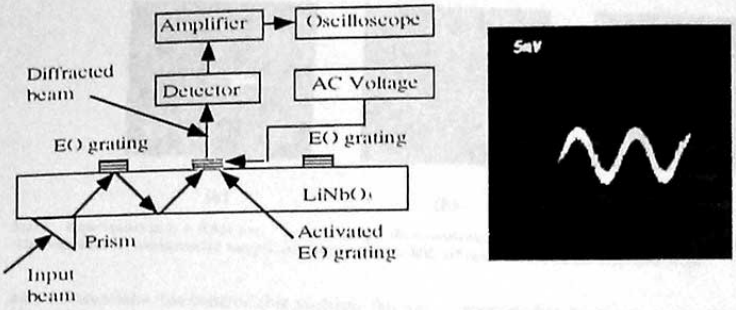

Fig. 7. Experimental setup for the evaluation of the EO thin phase grating array: (a) the setup, (b) modulation transfer curve represents $18 \pm 2.5°$ ($f = 60$ Hz).

is used to read data and an imaging lens is used in the reconstruction.

The real device under investigation is shown in Fig. 8(c), where a linear EO grating array with the associated elements is shown clearly. The EO grating activating the reference beam is switched on through the two microprobes shown in Fig. 8(c). In the experiment of the holographic write/read, a Fourier transform lens with a f-number of 2.0 is used. The size of input image of a bird pattern, as shown in Fig. 9(a), is 7.68 mm × 7.68 mm and contains 256 × 256 bits defined by a LCD. We obtain two reconstructed images at $\lambda = 0.633$ μm. Figure 9(b) shows the reconstructed image with the use of the second diffraction order (−50° diffraction angle) as the reference beam, and Fig. 9(c) makes use of the fifth diffraction order (−20°) as the reference beam. Note that these two reconstructed images have different qualities because they were made in two different write angles. Here, although we selected only two diffraction orders as the reference beams to carry out holographic recording and reading at one location, it is possible to implement the multiangle write/read at one location, i.e., the angle-multiplexing holographic write/read. For implementing the angle-multiplexing holographic write/read, the electro-optically controlled rotation switch array should be used to select the reference beam from all the diffraction orders with different angles (this device is omitted in Fig. 8). In accordance with the angle sensitivity of Dupont photopolymer film, this scheme can realize the angle-multiplexing holographic memory. On the other hand, although the experimental results were obtained at one wavelength ($\lambda = 0.633$ μm), the other wavelengths can also be used, so it is possible to implement the multiwavelength memory with the use of a tunable laser in accordance with the wavelength sensitivity of Dupont photopolymer film.

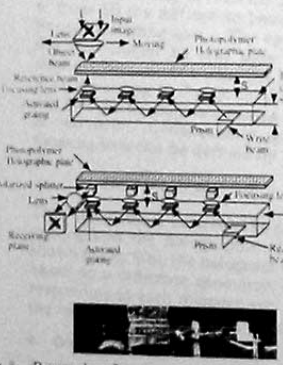

Fig. 8. Proposed configuration for hologram recording: (a) schematic for hologram recording, (b) schematic for hologram reading, (c) picture of a real device.

Typical forms of space-division schemes for the hologram multiplexing are the shift multiplexing and the angle multiplexing.[8–13] Almost all the angle-multiplexing schemes are based on the rotations of some devices that can change the angles of the reference beams. The angle-multiplexing scheme based on the mechanical rotation is generally limited by signal-to-noise ratio, the range of angles that can pass through the aperture of the optical system in the reference arm, and the numerical aperture or f-number of the imaging lens as well as the signal-to-noise ratio and the exposing angular sensitivity of the given holographic films. Hence the maximum number of holograms that can be angularly multiplexed at each location is less than ten.[13] According to the

(a) (b) (c)

Fig. 9. Experiments at $\lambda = 0.633$ μm: (a) input image, (b) reconstructed holographic image with the second diffraction order as the reference beam, (c) reconstructed holographic image with the fifth diffraction order as the reference beam.

above discussions, the controllable multiple fan-out of the EO grating consists of different diffraction angles, so the use of the different orders is equivalent to angle-multiplexing. This kind of angle-multiplexing scheme is limited by neither the range of angles that can pass through the aperture of the optical system in the reference arm nor the numerical aperture of the imaging lens. In this scheme the maximum number of holograms that can be angularly multiplexed at each location is directly equivalent to the maximum number of diffraction orders that can be used to make the multiplexing holograms. In addition, as shown in Fig. 8, we can effectively control the reference beam at different locations of the hologram plate by activating the corresponding EO grating so a nonmechanical shift multiplexing for the reference beam is also included in this scheme. If the thickness of the $LiNbO_3$ guided-wave substrate is t, the center-to-center distance between two adjacent EO gratings, i.e., the shift of the reference beam in each bouncing, should be $2t$ because the bouncing angle within the $LiNbO_3$ substrate is approximately 45°.

The signal beam has to be delivered at different locations, however. As shown in Fig. 8(a), a focusing lens corresponding to each EO grating has to be used to focus all the diffraction beams to one diffraction-limited recording spot. The aperture D of the focusing lens should be less than the center-to-center distance between two adjacent EO gratings (i.e., $D \leq 2t$). According to Fig. 5, the diffraction orders that can be used as reference beams are within the range of −60° to 0°. Consequently, the focal length f of the focusing lens can be defined by

$$D/2f = \tan 30° \quad \text{or} \quad f = (\sqrt{3}/2)D. \tag{15}$$

Thus the distance between the top surface of the EO grating and the holographic plate is $S = 2f$. As shown in Fig. 8(b), the hologram write–read system is based on a reflection geometry: a beam splitter corresponding to each memory spot is needed to obtain the reconstruction of holographic images.

4. Conclusions

A new architecture for implementing spatially multiplexed multiwavelength programmable holographic memory has been proposed. This architecture combines the guided-wave and free-space interconnects for controlling the reference and object beams, respectively. Although this architecture has not implemented a complete holographic recording and reading with no moving parts, the EO guided-wave interconnect technology has been applied to wavelength-multiplexing holographic memory. As a multiple fan-out device, the EO phase grating is studied in detail and an EO modulation efficiency of 18 ± 2.5% under an applied voltage of 100 V is obtained at $\lambda = 633$ nm. This is well matched with theoretical calculations. The experimental results obtained in this study verify the effective combination of free-space and guided-wave optical interconnects for spatial multiplexing multiwavelength holographic memory. In particular, the use of the multiorder diffracted beams of EO phase grating can implement the angle-multiplexing holographic storage as well as activate the reconfigurable reference beams. Although our experiments were performed for one wavelength, it is feasible to implement the multiwavelength memory if a tunable laser is used. Here the guided-wave travel of the reference beams within the linear EO grating array and the mechanical movement of the object beams can be used to select the different locations of the hologram plate for successively recording the holographic images, and at each location the no-moving-part overlapping holographic recordings can be implemented with the angle multiplexing and the wavelength multiplexing, respectively.

The authors thank T. C. Lee, Huajun Tang, and Chunhe Zhao for their help with this study.

References

1. R. T. Chen, H. Lu, D. Robinson, and T. Jannson, "Highly multiplexed graded-index polymer waveguide hologram for near-infrared eight-channel wavelength division demultiplexing," Appl. Phys. Lett. **59**, 1144–1146 (1991).
2. A. A. Rizvi and M. S. Zubairy, "Implementation of associative memory using grating structures," Appl. Opt. **33**, 3642–3646 (1994).
3. R. T. Chen, H. Lu, D. Robinson, M. Wang, G. Savant, and T. Jannson, "Guided-wave planar optical interconnects using highly multiplexed polymer waveguide holograms," IEEE J. Lightwave Technol. **10**, 888–897 (1992).
4. E. Arons and D. Dilworth, "Analysis of Fourier synthesis ho-

lography for imaging through scattering materials," Appl. Opt. **34**, 1841–1847 (1995).
5. G. A. Rakuljic, V. Leyva, and A. Yariv, "Optical data storage by using orthogonal wavelength-multiplexed volume holograms," Opt. Lett. **17**, 1471–1473 (1992).
6. S. Yin, H. Zhou, F. Zhao, M. Wen, Z. Yang, J. Zhang, and F. S. T. Yu, "Wavelength multiplexed holographic storage in a sensitive photorefractive crystal using a visible-light tunable diode laser," Opt. Commun. **101**, 317–321 (1993).
7. H. Zhou, F. Zhao, and F. S. T. Yu, "Effects of recording-erasure dynamics of storage capacity of a wavelength-multiplexed reflection-type photorefractive hologram," Appl. Opt. **33**, 4339–4344 (1994).
8. S. Campbell, X. Yi, and P. Yeh, "Hybrid sparse-wavelength angularly multiplexed optical data storage system," Opt. Lett. **19**, 2161–2163 (1994).
9. S. Campbell and P. Yeh, "Sparse-wavelength angle-multiplexed volume holographic memory system: analysis and advances," Appl. Opt. **35**, 2380–2388 (1996).
10. S. Tao, Z. H. Song, D. R. Selviah, and J. E. Midwinter, "Spatioangular-multiplexing scheme for dense holographic storage," Appl. Opt. **34**, 6729–6737 (1995).
11. F. H. Mok, "Angle-multiplexed storage of 5000 holograms in lithium niobate," Opt. Lett. **18**, 915–917 (1993).
12. D. Psaltis, M. Levene, A. Pu, G. Barbastathis, and K. Curtis, "Holographic storage using shift multiplexing," Opt. Lett. **20**, 782–784 (1995).
13. G. Barbastathis, M. Levene, and D. Psaltis, "Shift multiplexing with spherical reference waves," Appl. Opt. **35**, 2403–2417 (1996).
14. C. Denz, G. Pauliat, G. Roosen, and T. Tschudi, "Volume holographic multiplexing using a deterministic phase encoding technique," Opt. Commun. **85**, 171–176 (1991).
15. C. Alves, G. Pauliat, and G. Roosen, "Dynamic phase-encoding storage of 64 images in $BaTiO_3$ photorefractive crystal," Opt. Lett. **19**, 1894–1896 (1994).
16. K. Curtis and D. Psaltis, "Cross talk for angle- and wavelength-multiplexed image plane holograms," Opt. Lett. **19**, 1774–1776 (1994).
17. K.-H. Tu, T. Tamir, and H. Lee, "Multiple-scattering theory of wave diffraction by superposed volume gratings," J. Opt. Soc. Am. A **7**, 1421–1435 (1990).
18. A. Belendez, I. Pascual, and A. F. Fimia, "Model for analyzing the effects of processing on recording material in thick holograms," J. Opt. Soc. Am. A **9**, 1214–1223 (1992).
19. M. G. Moharam and T. K. Gaylord, "Three-dimensional vector coupled-wave analysis of planar-grating diffraction," J. Opt. Soc. Am. **73**, 1105–1112 (1983).
20. V. Minier and J. M. Xu, "Coupled-mode analysis of superimposed phase grating guided-wave structures and integrating coupling effects," Opt. Eng. **32**, 2054–2063 (1993).
21. T. Kubota and M. Takeda, "Array illuminator using grating couplers," Opt. Lett. **14**, 651–652 (1989).
22. R. T. Chen, D. Robinson, H. Lu, M. R. Wang, T. Jannson, and R. Baumbick, "Reconfigurable optical interconnection network for multimode optical fiber sensor arrays," Opt. Eng. **31**, 1098–1106 (1992).
23. A. Pu and D. Psaltis, "High-density recording in photopolymer-based holographic three-dimensional disk," Appl. Opt. **35**, 2389–2398 (1996).
24. E. N. Glytsis and T. K. Gaylord, "Anisotropic guided-wave diffraction by interdigitated electrode-induced phase gratings," Appl. Opt. **27**, 5031–5050 (1988).
25. D. G. Sun, C. Zhao, and R. T. Chen, "Intraplane to interplane optical interconnects with a high diffraction efficiency electro-optic grating," Appl. Opt. **36**, 629–634 (1997).
26. M. C. Hutley, *Diffraction Gratings* (Academic, New York, 1982).
27. A. Yariv and P. Yeh, *Optical Waves in Crystals* (Wiley, New York, 1984).